Mitigation of Tropospheric InSAR Phase Artifacts Through Differential Multisquint Processing

Curtis W. Chen

Jet Propulsion Laboratory, California Institute of Technology
4800 Oak Grove Dr.
Pasadena, CA 91109-8099

Abstract **We propose a technique for mitigating tropospheric phase errors in repeat-pass interferometric synthetic aperture radar (InSAR). The mitigation technique is based upon the acquisition of multisquint InSAR data. On each satellite pass over a target area, the radar instrument will acquire images from multiple squint (azimuth) angles, from which multiple interferograms can be formed. The diversity of viewing angles associated with the multisquint acquisition can be used to solve for two components of the 3-D surface displacement vector as well as for the differential tropospheric phase. We describe a model for the performance of the multisquint technique, and we present an assessment of the performance expected.**

I. INTRODUCTION

Tropospheric phase artifacts may be a dominating source of error in repeat-pass interferometric synthetic aperture radar (InSAR) measurements [1, 2]. These phase errors arise mainly from the spatial and temporal variability of water vapor in the troposphere, which affects the effective path lengths experienced by the radar pulses. In a single repeat-pass interferogram, these troposphere-induced variations in path length are indistinguishable from the true surface displacements under investigation.

Here, we propose a technique for mitigating tropospheric phase errors in repeat-pass interferometry. The mitigation technique is based upon the acquisition of multisquint InSAR data. That is, on each satellite pass over a target area on the ground, the radar instrument will acquire images from multiple squint (azimuth) angles. With such data from two or more passes, multiple interferograms corresponding to the different squint angles can be formed. Because each interferogram is sensitive only to the line-of-sight component of the surface displacement and the local tropospheric delay, the diversity of viewing angles associated with the multisquint acquisition can be used to solve for two components of the 3-D surface displacement vector as well as for the differential tropospheric phase that would otherwise corrupt a two-pass interferometric measurement.

In the remainder of this paper, we first describe a simplified model for the performance of the multisquint technique, then we present an assessment of the expected performance of the technique assuming a reasonable set of system parameters.

II. Multisquint Tropospheric Phase Mitigation

In this section, we describe the multisquint technique in terms of a simple system model which includes only first-order tropospheric effects. For simplicity, we assume a flat-Earth geometry in which the platform follows a straight-line flight path. We also assume that the platform flight track repeats itself exactly so that there is no interferometric phase dependence on the surface topography. For the moment, we assume that the troposphere acts as a thin phase screen at zero altitude.

For a single repeat-pass interferogram, the observed interferometric phase ϕ_{obs} is composed of components due to (1) the true surface displacement, (2) the tropospheric path delay to be removed, and (3) noise. While the true surface displacement is described by a vector in 3-D space, the interferometric phase is sensitive only to the projection of this vector onto the line of sight from which the data were acquired. Over the set of possible squint angles along a single satellite pass over a fixed target area on the ground, the various platform-to-target lines of sight define a plane, referred to as the slant plane, oriented at an angle θ_l (the instrument look angle) from vertical. Let ρ_0 be the slant range to the target area at closest approach, and let θ_{sq} be the squint angle as shown in Fig. 1. The observed interferometric phase is then given by

$$\phi_{\text{obs}} = -\frac{4\pi}{\lambda}\left(\delta_x \sin\theta_{\text{sq}} + \delta_y \cos\theta_{\text{sq}} + \delta_{\text{atm}}\frac{1}{\cos\theta_{\text{sq}}}\right) + \phi_{\text{noise}} \tag{1}$$

where δ_x and δ_y are the slant-plane components of the 3-D surface displacement vector parallel and perpendicular to the platform flight track, δ_{atm} is the apparent displacement due to the tropospheric path delay to be removed, and λ is the system wavelength. The sine and cosine terms

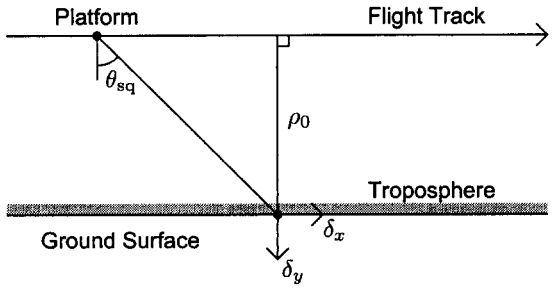

Figure 1: Geometry for the model used to describe the performance of the multisquint technique. The plane of the page corresponds to the slant plane.

multiplying the surface-displacement components δ_x and δ_y project the surface-displacement vector onto the radar line of sight. (Note that y is not the ground-range coordinate here.) The cosine term multiplying the tropospheric path delay δ_{atm} is an obliquity factor that accounts for the longer slant path through the troposphere at higher squint angles. We assume that the interferogram is well correlated and that multiple looks have been taken such that the phase noise is approximately Gaussian with zero mean and variance σ_n^2.

Suppose that on each satellite pass over the target area, N images are acquired at the set of squint angles contained in the vector $\vec{\theta}_{\text{sq}}$. With two passes worth of data, one interferogram can be formed for each squint angle, giving a total of N interferograms. The vector $\vec{\phi}_{\text{obs}}$ of observed interferometric phase data for a single ground point is then given by

$$\vec{\phi}_{\text{obs}} = -\frac{4\pi}{\lambda}\mathbf{A}\begin{bmatrix} \delta_x \\ \delta_y \\ \delta_{\text{atm}} \end{bmatrix} + \vec{\phi}_{\text{noise}} \tag{2}$$

where the $N \times 3$ matrix $\mathbf{A}$ is defined as

$$\mathbf{A} = \begin{bmatrix} \sin\vec{\theta}_{\text{sq}} & \cos\vec{\theta}_{\text{sq}} & \frac{1}{\cos\vec{\theta}_{\text{sq}}} \end{bmatrix} \tag{3}$$

and $\vec{\phi}_{\text{noise}}$ is a vector of N independent, identically distributed (IID) phase noise terms. In Eq. (2), the δ terms correspond to a particular ground location under observation and can vary over the scene. These terms are assumed to remain temporally constant over an individual satellite pass, however, so they are identical for each of the N images in the pass. The term δ_{atm} is the differential tropospheric path delay between the two passes comprising the data set (at the specified ground location).

The key idea of the multisquint technique is based on the observation that, noise nothwithstanding, Eq. (2) contains three unknowns (δ_x, δ_y, δ_{atm}) for each ground location, while the number of equations N can be made greater than or equal to three by acquiring data from at least three squint angles. Therefore, for $N \geq 3$, Eq. (2) may be inverted to obtain the least-squares estimates $\hat{\delta}_x$, $\hat{\delta}_y$, and $\hat{\delta}_{\text{atm}}$ of the slant-plane surface-displacement components and the differential tropospheric path delay:

$$\begin{bmatrix} \hat{\delta}_x \\ \hat{\delta}_y \\ \hat{\delta}_{\text{atm}} \end{bmatrix} = -\frac{\lambda}{4\pi}\left(\mathbf{A}^{\text{T}}\mathbf{A}\right)^{-1}\mathbf{A}^{\text{T}}\vec{\phi}_{\text{obs}}. \tag{4}$$

Define the $3 \times N$ matrix $\mathbf{H}$ as

$$\mathbf{H} = -\frac{\lambda}{4\pi}\left(\mathbf{A}^{\text{T}}\mathbf{A}\right)^{-1}\mathbf{A}^{\text{T}}. \tag{5}$$

Equation (4) then becomes

$$\begin{bmatrix} \hat{\delta}_x \\ \hat{\delta}_y \\ \hat{\delta}_{\text{atm}} \end{bmatrix} = \mathbf{H}\vec{\phi}_{\text{obs}}. \tag{6}$$

By our assumption of IID zero-mean noise with variance σ_n^2, the expected error on each of the least-squares estimates $\hat{\delta}_x$, $\hat{\delta}_y$, and $\hat{\delta}_{\text{atm}}$ is given by the root sum square of the elements on the corresponding row of $\mathbf{H}$. If the true displacement and tropospheric path delay terms are spatially stationary over a local neighborhood, the estimate error can be reduced by spatial averaging (*i.e.*, taking looks). The improvement in performance is then proportional to the square root of the number of looks N_L. The expected error variances σ_x^2, σ_y^2 and σ_{atm}^2 of the least-squares estimates $\hat{\delta}_x$, $\hat{\delta}_y$, and $\hat{\delta}_{\text{atm}}$ are thus given by

$$\begin{bmatrix} \sigma_x^2 \\ \sigma_y^2 \\ \sigma_{\text{atm}}^2 \end{bmatrix} = \frac{\sigma_n^2}{N_L}\left(\mathbf{H}\cdot\mathbf{H}\right)\vec{1} \tag{7}$$

where "$\cdot$" represents the Hadamard product, or element-wise multiplication, and $\vec{1}$ represents an N-length vector whose elements are all unity. The expression $(\mathbf{H}\cdot\mathbf{H})\vec{1}$ therefore represents a squaring of the elements of $\mathbf{H}$ and a summation of the rows of the result. The error standard deviations σ_x, σ_y and σ_{atm} are simply the square roots of the error variances given above. Values for the expected errors with potential system parameters are given in Section IV.

III. Spatial and Temporal Variation Effects

The model of the previous section assumes that the troposphere is locally stationary and confined to a thin layer just above the ground surface, and that it remains static over the time required for the N images of a single pass to be acquired. This model might lead to overly optimistic expectations for the performance of the multisquint technique in many situations, however, as the real behavior

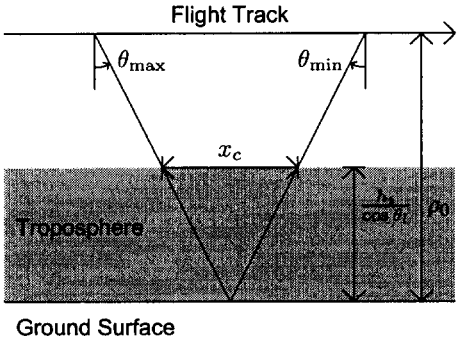

Figure 2: Geometry for computing the ray-path separation x_c at the effective top of the troposphere. The plane of the page represents the slant plane, oriented at an angle θ_l from vertical.

of the troposphere is characterized by both spatial and temporal variability. While a detailed discussion of such effects is beyond the scope of this paper, we provide an overview of the relevant issues in this section.

While most of the tropospheric water vapor responsible for InSAR phase artifacts is indeed confined to a relatively thin (approximately 2 km) layer close to the ground [1], the thin-screen approximation of the previous section is inadequate because it fails to model the fact that ray paths from a given target to various points along the platform flight track travel through different parts of the troposphere and consequently experience different overall path delays. The correlation between the total path delay values for the two rays decreases as the effective height of the troposphere increases. The correlation also decreases as the difference in squint angle between the two rays increases.

For the purposes of this analysis, we adopt the following highly simplified model. Let x_c be the lateral ray-path separation at the effective height h_t of the troposphere between rays corresponding to the maximum and minimum squint angles $\theta_{\max}$ and $\theta_{\min}$ of the acquired data (see Fig. 2):

$$x_c = \frac{h_t}{\cos\theta_l} \left| \tan\theta_{\max} - \tan\theta_{\min} \right| . \tag{8}$$

We assume that for horizontal spatial scales smaller than x_c, the tropospheric path delays exhibited at different squint angles are completely uncorrelated, while for spatial scales larger than x_c, the delays are completely correlated.

Just as high-frequency spatial variations in tropospheric water vapor content cannot be removed with the multisquint technique, high-frequency temporal variations will lead to residual errors as well. The assumption made in Eq. (2) is that the tropospheric errors remain correlated over the time needed to acquire the N images of a single satellite pass. The need for temporal correlation over the N data sets is, of course, also the reason that the N images cannot be acquired on different passes.

Here, we adopt a model that relates the temporal variations of the troposphere to its spatial variations in order to estimate the level of residual errors due to changes in the troposphere during the time required for single-pass data acquisition. That is, we adopt the "frozen-flow hypothesis," which assumes that the atmosphere can be modeled as an internally static slab that, carried by the wind, passes over the ground at a constant velocity.

Let t_{acq} be the time required for the instrument to collect the N multisquint images of a single pass. Based on Fig. 2,

$$t_{\text{acq}} = \frac{\rho_0 \left| \tan\theta_{\max} - \tan\theta_{\min} \right|}{v_{\text{plat}}} \tag{9}$$

where v_{plat} is the platform velocity. During the time t_{acq}, the frozen atmosphere slab therefore moves by an amount x_w, given by

$$x_w = t_{\text{acq}} v_{\text{wind}} . \tag{10}$$

We then use the value of x_w as we did the value of x_c.

IV. Expected Performance

In order to model the expected performance of the multisquint technique, we henceforth assume a data acquisition scenario in which three SAR images of the target ground area are acquired per satellite pass ($N = 3$), at squint angles $+\theta_0$, 0, and $-\theta_0$. We will examine cases for which $\theta_0 = 15°$ and $\theta_0 = 30°$, assuming the spaceborne scenario of Table 1. For a spacecraft, modifications to the flat-Earth model might be necessitated by the curvature of the orbit track. This issue is not addressed here, however.

For the noise standard deviation σ_n, we assume a value equivalent to 5 mm RMS line-of-sight displacement accuracy per single interferogram at a spatial posting Δ_{int} of 100 m. This noise term includes the effects of thermal noise, temporal decorrelation of the surface between passes, volumetric decorrelation, residual ionospheric errors, and residual high-frequency tropospheric path delay errors. We assume that 400 spatial looks have been averaged to result in an output product with a posting Δ_{msq} of 2 km. This posting was chosen so as to approximately match the scale sizes x_w and x_c, which are conveniently similar to one another for the system parameters used here. Note that for simplicity, we have assumed a fixed level of residual high-frequency tropospheric errors that is the same for the two squint cases, although in reality, the residual error level would depend upon the chosen squint angles. The assumed parameters are summarized in Table 1.

Platform altitude	h_{plat}	760 km
Platform velocity	v_{plat}	7500 m/s
Broadside slant range	ρ_0	850 km
Broadside look angle	θ_l	25°
Radar wavelength	λ	24 cm
Antenna length	L	14 m
Antenna footprint width	W_f	15 km
Synthetic aperture length	L_{SA}	15 km
Displacement error	σ_n	5 mm
Interferogram posting	Δ_{int}	100 m
Number of squint angles	N	3
Number of multisquint looks	N_L	400
Multisquint product posting	Δ_{msq}	2000 m
Effective troposphere height	h_t	2000 m
Effective wind speed	v_{wind}	10 m/s

Table 1: Summary of assumed system and environment parameters used for performance evaluation assuming three acquisitions per satellite pass at squint angles of $+\theta_0$, 0, and $-\theta_0$.

		$\theta_0 = 15°$	$\theta_0 = 30°$
x_c	(m)	1200	2500
x_w	(m)	600	1300
t_{acq}	(s)	61	131
σ_x	(mm)	0.7	0.4
σ_y	(mm)	4.5	1.2
σ_{atm}	(mm)	4.3	1.0

Table 2: Summary of performance parameters assuming three acquisitions per satellite pass at squint angles of $+\theta_0$, 0, and $-\theta_0$, with the assumed parameters of Table 1.

Based on Eq. (7), the expected performance results for the parameters described above are summarized in Table 2. The results suggest that surface-displacement accuracies on the order of a few millimeters or better are possible at postings on the order of 2 km with use of the multisquint technique. The displacement accuracies scale linearly with σ_n and almost inversely with $\sqrt{N_L}$.

Figure 3 illustrates the dependence of the error terms σ_x, σ_y, and σ_{atm} on the value of θ_0 for the example scenario above. Once again, the value of σ_n has been kept fixed at 5 mm for all cases. A knee in the curve is apparent around values of $\theta_0 \approx 15$–$20°$.

V. CONCLUSIONS

We have described a technique for mitigating tropospheric path-delay artifacts in repeat-pass interferograms. The technique relies on only two satellite passes, so science results might be obtained in a much more timely manner than would be possible if many interferograms were to be averaged to reduce tropospheric effects. The technique will likely be capable of producing results only at relatively coarse (kilometer-scale) resolutions, however.

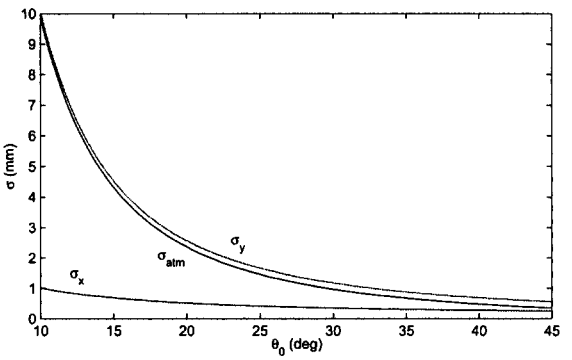

Figure 3: RMS displacement error and tropospheric path delay error for various values of θ_0 with the same system parameters assumed for Table 1. Note that σ_n has been kept fixed for all values of θ_0.

While intuition might suggest that the technique requires at least three times as long to acquire global maps because of the threefold decrease in the ground coverage area per pass, this is not necessarily the case. From each multisquint data set, two components of the surface displacement are computed, so the coverage of the technique is lessened only by a factor of 1.5. Furthermore, because the multisquint technique might obviate the need for stacking, the technique might actually result in more useful science data.

Although the analysis presented here shows promise for the technique, it should be noted that this analysis is preliminary and based upon a number of simplifications and assumptions. Further verification and/or refinement of these assumptions would comprise a logical subject for future work.

ACKNOWLEDGMENT

This work was performed at the Jet Propulsion Laboratory, California Institute of Technology, under contract with NASA.

REFERENCES

[1] R. F. Hanssen, *Radar Interferometry: Data Interpretation and Error Analysis*, (Kluwer Academic Publishers, Dordrecht, 2001).

[2] H. A. Zebker, P. A. Rosen, and S. Hensley, "Atmospheric Effects in Interferometric Synthetic Aperture Radar Surface Deformation and Topography Maps," *Journal of Geophysical Research*, **102**, 7547–7563 (1997).